Static Uniaxial Compression of Polyisoprene–Montmorillonite Nanocomposites Monitored by ^{1}H Spin–Lattice Relaxation Time Constants

G. M. Poliskie,[1] R. E. Cohen,[2] K. K. Gleason[2]

[1]*Department of Materials Science and Engineering, Massachusetts Institute of Technology, Cambridge, Massachusetts 02139*
[2]*Department of Chemical Engineering, Massachusetts Institute of Technology, Cambridge, Massachusetts 02139*

Received 7 June 2004; accepted 1 March 2005
DOI 10.1002/app.22328
Published online in Wiley InterScience (www.interscience.wiley.com).

ABSTRACT: Previous work has focused on the use of microscopy to explore the mechanisms of deformation in polymer nanocomposites. That technique creates a qualitative representation that may not be statistically representative of the bulk properties. This paper illustrates the utility of solid-state NMR, which inherently measures bulk behavior, to both identify and quantify mechanisms of deformation. Specifically, in this study, increases in the interfacial area of various modifications of Cloisite clay in 1,4-*cis* polyisoprene nanocomposites were monitored during uniaxial compression. Interaction of the Fe^{+3} in the clay with the polymer decreases the polymer's ^{1}H spin–lattice relaxation time constant (T_1). In some of the nanocomposites, the increase in the interfacial area of the clay platelets was observed by a decrease in the polymer's T_1 with successive amounts of strain. The observation of these changes with static ^{1}H-NMR is limited by the dispersion of the clay. © 2005 Wiley Periodicals, Inc. J Appl Polym Sci 98: 1806–1813, 2005

Keywords: compression; NMR; polyisoprene; clay

INTRODUCTION

Transmission electron microscopy (TEM) of elongated nylon-6 montmorillonite composites indicated that individual clay layers of the aggregate could be pulled apart with macroscopic tensile strain.[1] TEM allows for the qualitative observation of microscopic deformation; however, each individual micrograph is not necessarily representative of the bulk composite. Furthermore, to quantitatively determine changes in the interfacial area between the clay and the polymer, multiple micrographs would have to be taken over the entire sample. In contrast, NMR is a technique that inherently averages the bulk properties of the composite. Therefore, it is useful to explore the utility of NMR to identify and quantify this mechanism of deformation in polymer nanocomposites.

Polyisoprene and polyisoprene composites have been the subject of a large number of studies aimed at improving their mechanical properties due to their widespread industrial uses.[2–8] In particular, clay nanocomposites have found a niche in the automotive and sporting goods industries.[9] Clay has an advantage over traditional fillers due to their larger aspect ratio, which allows for more interfacial contact with the polymer. As a result of this higher aspect ratio, a clay nanocomposite has the capability of improving strength with lower loadings than that used for traditional composites.[9]

NMR has recently been used not only to identify structural changes in the polymer, but also to determine how these changes influence the macroscopic mechanical properties. *In situ* and quasistatic experiments on a number of semicrystalline and elastomeric polymers have explored the changes in structure as a function of stress or strain.[10–13] Little work has focused on the mechanical and structural effects of the addition of montmorillonite clay to polyisoprene. What has been reported has focused on the well-dispersed, surface-modified clay in a crosslinked polyisoprene matrix.[14–16] NMR work on composites has been limited to studies of the structural changes of the matrix polymer upon the addition of clay.[17–19] Since polyisoprene is an elastomeric and not a semicrystlalline polymer, the addition of clay should not significantly alter the morphology of the matrix. Furthermore, no NMR *in situ* mechanical measurements have been reported on clay-filled polyisoprene nancomposites. Therefore, this study investigates the use of NMR to better understand the behavior of uncrosslinked polyisoprene nanocomposites under deformation. Understanding this behavior will aid in optimizing the

Correspondence to: K. K. Gleason (kkg@mit.edu).
Contract grant sponsor: U.S. Air Force; contract grant number: F49620–01-1–0447.

design of a mechanically desirable polyisoprene nanocomposite. Furthermore, this study will illustrate the utility of solid-state NMR to quantitate changes in the interfacial area between the clay and polyisoprene when the composite is deformed.

EXPERIMENTAL

Aldrich 97% *cis* 1,4-polyisoprene with weight average molecular weight 800,000 g/mol was used as received. Cloisite, a montmorillonite clay with varying surfactant modifications, was purchased from Southern Clay Products. The surfactants on the clays included methyl, tallow, bis-2-hydroxyethyl quaternary ammonium (30B), dimethyl, dehydrogenated tallow quaternary ammonium (20A), and dimethyl, hydrogenated tallow, 2-ethylhexyl quaternary ammonium (25A). All blends were solvent cast from a 1.1 wt % solution of polyisoprene in THF to which was added 0.15 wt % of the corresponding clay. After solvent evaporation, the clay made up 13 wt % of the polymer nanocomposite. For those blends that contained varying amounts of Na^+ exchanged clay, the solution of polyisoprene in THF remained 1.1 wt % and the solution of clay consisted of 0.23, 0.34, and 0.45 wt % to make 20, 30, and 40 wt % blends upon solvent evaporation, respectively.

Wide-angle X-ray diffraction (WAXD) measurements were made on a Riguku Ru300 X-ray generator with Cu Kα radiation. The operating voltage was 60 kV with a current of 300 mA. Spectra were taken, from thin films cast upon glass sides, in reflection mode at room temperature.

TEM was performed on a Joel 2000FX instrument. This instrument had a lanthanum filament operating at 200 kV. Samples were cryomicrotomed at -130 °C to a thickness of 50 nm using a MT-X Ultramicrotome and a diamond knife. The samples were collected on 400 mesh copper grids.

The mechanical data were acquired with an Instron Model No. 4201 operated in compression mode at room temperature. The specimens were rectangular with dimensions: $0.2 \times 0.2 \times 0.4$ in. Both the top and the bottom of the polymer specimen had a Teflon–polymer interface allowing for equal slip on both sides. The deformation rate was 0.5 mm/min. A 5-kN compression load cell was used for all tests.

All NMR spectra were taken with an Oxford 6.3-T magnet (with a 270-MHz ^{1}H resonance frequency) using a Tecmag dual-resonance pulse generator and receiver. Static ^{1}H experiments were performed on a homebuilt probe with a 2-μs $\pi/2$ pulse width. Spectra were acquired with a 10-μs dwell time and a 5-s recycle delay. The static spectra, represented in Figure 3, were taken at room temperature and the spin–lattice relaxation times were taken at -10 °C (± 1 °C), unless otherwise noted. The nanocomposites were compressed at room temperature and then the temperature was decreased for NMR acquisition. These spectra were taken after a 10-min wait for temperature equilibration and stress relaxation. The lower temperature was regulated with a N_2 gas stream submerged in a dewar containing liquid N_2.

The device used for static spectra in the presence of compressive strains was a Teflon rod 0.25 in. in diameter and 1.00 in. in length. The polymer was placed in a threaded 0.18-in.-diameter hole and compression was induced by successive turns of the nylon screw. A Teflon spacer between the polymer and screw allowed for slip at one end of the specimen while the bottom of the Teflon device created slip at the other. Accordingly, the polymer specimens were rectangular with the dimensions of $0.09 \times 0.09 \times 0.30$ in. After 40% compressive strain, there was clearance between the specimen's circumference and the sides of the compression cell.

Spin–lattice relaxation time constants were measured using an inversion recovery sequence (π–τ_d–$\pi/2$–Acq). A single least-square exponential was fitted to the peak intensity (M) versus delay time (τ), resulting in a two-parameter fit yielding the equilibrium peak intensity (M_0) and the spin–lattice relaxation time constant (T_1) (eq. 1).[20]

$$M(\tau) = M_o(1 - 2\exp(-\tau/T_1)) \quad (1)$$

Applying this single exponential for the nanocomposites resulted in an R^2 value ≥ 0.99 in all cases. Each fit consisted of 15 points from equally spaced delay times. All T_1 time constants are reproducible within 7% error. Simulations of line shapes for the static spectra were performed with the use of GRAMS software with three peaks used to represent the three chemically distinguishable protons. For the homopolymer, simulated peaks were Gaussian with the full width half mass (FWHM) line widths extracted from the simulation. A Lorentzian peak was used to simulate the line shape for the various nanocomposites.

RESULTS

There was no clear difference in the type of clay tactoids seen in the TEM as a function of surfactant modification. Representative micrographs from the blend with the 30B surfactant are presented in Figure 1. Figure 1(a) shows sheets of clay clustering in micron sized clumps. In Figure 1(b), single exfoliated clay sheets can be observed surrounding smaller clusters.

Figure 2 and Table I provide more quantitative details of the clay tactoids in the various blends. In Figure 2, shifts in the wide angle X-ray diffraction spectra indicate that there is some intercalation of polyisoprene chains into the galleries of the clay struc-

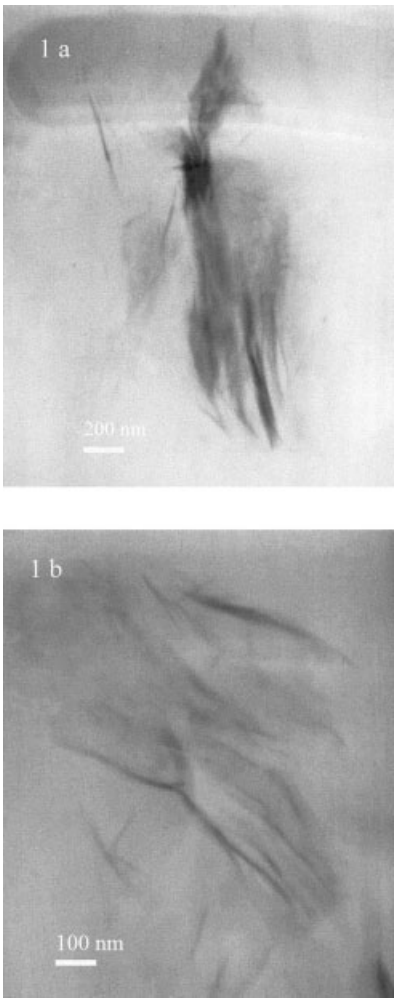

Figure 1 TEM images of the *cis* 1,4-polyisoprene blended with 13 wt % 30B montmorillonite prior to deformation.

ture, with the amount depending on the nature of the surfactant. The largest change in spacing shown in Table I indicates that surfactant 20A is the most compatible with polyisoprene.

Figure 3 is a representative static spectrum of polyisoprene with and without montmorillonite filler. The static spectrum of polyisoprene is resolved into the methine (a) resonance and the combined methylene (b) and methyl (c) resonances (see Fig. 4). In the case of the homopolymer, the FWHM was ~200 Hz for the methine resonance and ~400 Hz for the combined methyl and methylene resonance. The broadening in the presence of clay causes a loss of spectral resolution of the methine vs. the methylene and methyl protons and increases the FWHM. The linewidths of the nanocomposites cluster into the two groups consisting of the less polar surfactants 20A and 25A, FWHM ~ 3200 Hz, and the more polar surfactant 30B and Na^+ exchanged clay, FWHM ~ 2800 Hz.

Figure 5 is a plot of the inverse of the measured T_1 time constants vs. the weight percentage of Na^+ exchanged clay. The T_1 value decreased with increasing weight percentage of clay at both temperatures of −10 and 0 °C.

Figures 6 and 7 are the magnetization recovery plots at three different values of strain for the nanocomposites containing Na^+ exchanged and 30B surfactant, respectively. In the case of the Na^+ exchanged clay, there is a steady decrease in the T_1 from 0 to 40% strain. For the 30B surfactant containing nanocomposite, there is an initial drop in the T_1 at 20% strain but no further drop after 20%.

The T_1 time constants for all four *cis* 1,4-polyisoprene nanocomposites are represented in Figure 8. The initial value of T_1, prior to compression, is smaller for the less polar surfactants. The nanocomposites containing the two more polar surfactants, Na^+ and 30B, have the same initial T_1 of ~1 s and the two nanocomposites containing the less polar surfactant, 20A and 25A, have an initial T_1 of ~0.7 s. The nanocomposites containing Na^+ and 30B are the only samples showing a significant drop in T_1 with increasing compressive strain.

The addition of clay to polyisoprene had a statistically significant, but small, effect on the compression modulus as indicated in Figure 9. Specifically, there was a small drop in the compression modulus for the 20A and 25A modified nanocomposites.

DISCUSSION

Using solid-state NMR to determine changes in the interfacial area of the nanocomposite requires that the clay contain paramagnetic Fe^{+3} centers, which are used as markers. In addition, it requires that there be unexposed Fe^{+3} centers in the aggregate to observe changes with an increase in strain. Therefore, TEM and WAXD were used to differentiate composites with unintercalated aggregates, with unexposed paramagnetic centers, from composites in which extensive intercalation makes changes in interfacial area difficult to observe. Furthermore, the bulk macroscopic modulus was related to the microscopic architecture of the composite.

As seen in Figure 1, different sized clusters could be identified in the TEM in all specimens. Because a single platelet has dimensions of 1 to 75–100 nm,[21] the micrometer-sized aggregates must be composed of multiple platelets. It is important to establish the presence of aggregates, with unexposed clay surface area, to interpret the NMR as an increase in interfacial area during deformation.

Montmorillonite clay contains paramagnetic Fe^{+3} in its galleries; the Fe_2O_3 comprises 3.11–4.28 atomic weight percent of the clay depending on the source.[21] The presence of these paramagnetic centers has important implications for the acquisition of NMR spectra. The linewidth is inversely related to the inhomo-

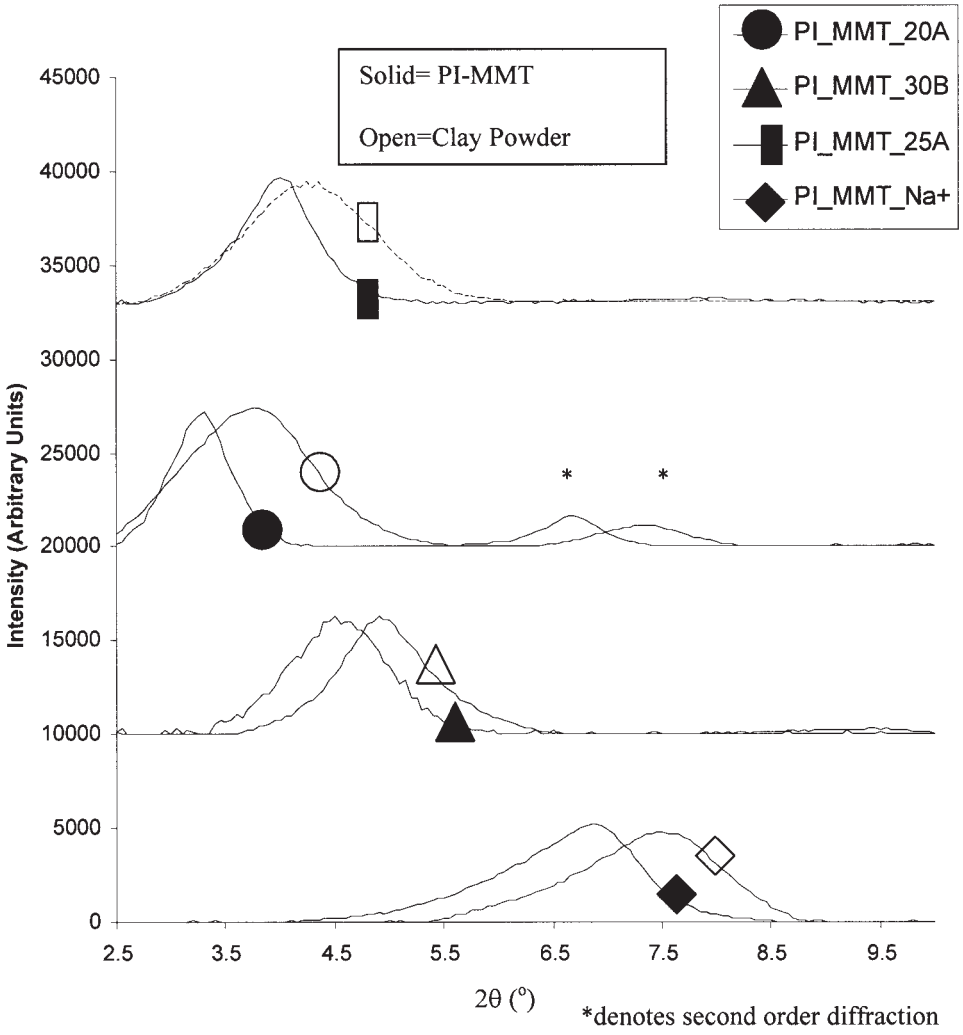

Figure 2 WAXD of *cis* 1,4-polyisoprene-montmorillonite nanocomposites.

geneous spin–spin relaxation, which is influenced by the homogeneity of the local magnetic field around the observed nucleus. As noted in other systems,[22,23] each paramagnetic center alters the local magnetic field around it, increasing the linewidth.[24] Figure 3 indicates that these local field gradients broaden the spectrum, decreasing the spectral resolution of chemically inequivalent nuclei. Because of the broadening, the T_1 time constants could not be assigned to a particular proton moiety. Instead the T_1 values describe the collective behavior of all the protons on the polymer.

TABLE I
Comparison of WAXD Spacing of *cis* 1,4-Polyisoprene–Montmorillonite Nanocomposites

Type of nanocomposite	Clay spacing (nm)	Nanocomposite spacing (nm)	Change in spacing (nm)
Na^+	1.16	1.28	0.12
30B	1.80	1.95	0.15
20A	2.35	2.68	0.33
25A	2.08	2.20	0.12

The nanocomposites with the nonpolar surfactants, 20A and 25A, are expected to disperse better in the polyisoprene matrix since their chemical structures more closely match that of the polymer. Consistent with this logic, these two composites had a larger FWHM due to the greater distortion of the local field created by the larger amount of exposed Fe^{+3} centers. This illustrates the utility of NMR to identify improved dispersions caused by adding the appropriately modified clay.

For the nanocomposites, the T_1 time constant is a linear combination of variety of factors which include, but are not limited to paramagnetic centers, dipolar coupling, and chemical shift anisotropy (eq. 2).[24]

$$1/T_1 = 1/T_{1\text{para}} + 1/T_{1\text{anisotropy}} + 1/T_{1\text{dipolar}} \quad (2)$$

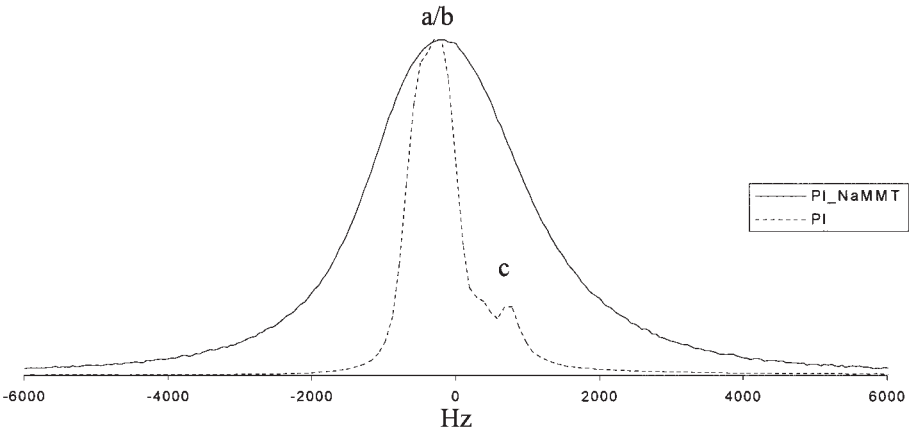

Figure 3 Static ^{1}H-NMR of *cis* 1,4-polyisoprene and *cis* 1,4-polyisoprene containing 13 wt % Na^+ exchanged montmorillonite.

The chemical shift anisotropy for protons is small;[25] therefore, the dipolar coupling and the paramagnetic effect are the two largest contributions to the T_1 parameter. The paramagnetic contribution for a system with spin diffusion has been worked out by others,[24,26] the spin–lattice relaxation can be related to the concentration of paramagnetic sites (N), the diffusion barrier length (b), and the spin diffusion constant (D) (eq. 3). Therefore, as the polymer is exposed to more Fe^{+3} centers (N), within the diffusion barrier of 0.5 nm,[27] the contribution from the paramagnetic effect will increase and the measured ^{1}H T_1 time constant of the polymer will decrease.

$$1/T_{1\text{para}} = 4\pi NbD \tag{3}$$

As has been cited by other authors[26–29] and according to eq. 3, a larger concentration of paramagnetic centers lowers the T_1 value. Figure 5 shows that T_1 decreases when the weight percent of clay increases, suggesting an increase in the amount of Fe^{+3} sites interacting with the polymer. The linear regression to the data, at −10 °C, in Figure 5 is presented in eq. (4).

$$1/T_{1\text{para}} = 0.030 \pm 0.002(\text{wt\% clay}) + 0.66 \pm 0.03 \tag{4}$$

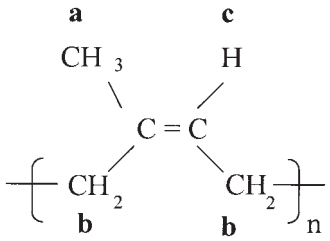

Figure 4 Structure of *cis* 1,4- polyisoprene.

The combination of eqs. (2) and (3) would create an equation of the same form as the linear regression (eq. 4). However, the theory presented in eq. (3) was developed for a homogenous distribution of paramagnetic centers with each center having a spherically symmetric interaction with neighboring spins.[24] For these composites, each paramagnetic center is embedded in the clay platelet. Those centers buried in the center of the aggregate will not influence the relaxation of the polymer's spins and those at the edges of the aggregate will only be surrounded by polymer on one or two sides, making their interaction with the polymer nonspherical. Therefore, this model cannot be rigorously used to find an absolute concentration of paramagnetic centers; however, it does provide the correct functional dependence to explain our observations and allows us to ratio the changes occurring as more paramagnetic centers are exposed to the spins.

Figures 6 and Figure 7 show that the T_1 decreases with an increase in compressive strain, suggesting an increase in the number of paramagnetic centers exposed to the polymer. This increase in number of exposed centers is likely the result of a deformation of the clay aggregates. As the aggregates break apart there is an increase in the interfacial area between the polymer and clay platelets.[1] The decrease in T_1 for the Na^+ exchanged nanocomposites after 40% of strain was ~0.30 s, which from linear fit of Figure 5 (eq. 4) corresponds to a 226% increase in interfacial area. For the 30B exchanged nanocomposites, the decrease was ~0.20 s, corresponding to a 173% increase in interfacial area. Furthermore, experiments indicated that when the strain is released the T_1 does not change from its value at 40% strain. Therefore, the increase in interfacial area is irreversible. This suggests that it is possible to improve the dispersion of the clay by shearing the mixture when the clay is blended into the polyisoprene.

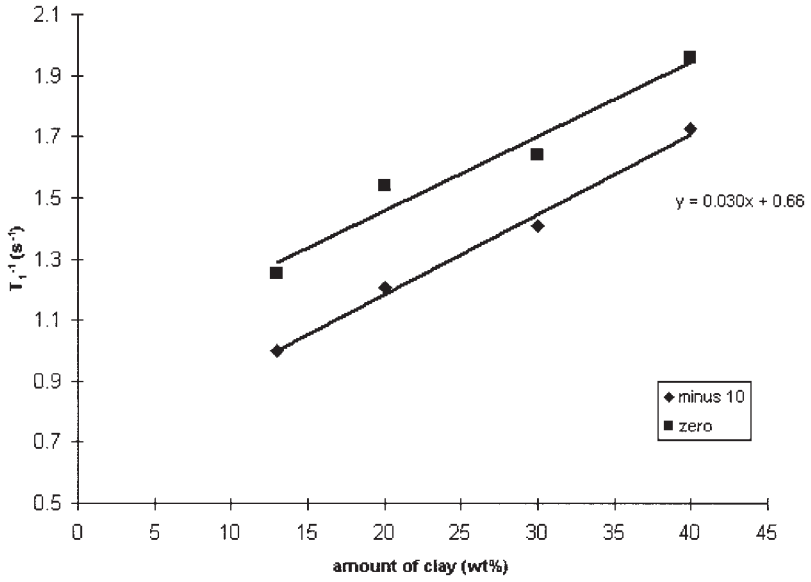

Figure 5 Plot of T_1 time constants as a function of amount of clay added for Na^+ exchanged clay nanocomposites.

Improving the dispersion of clay increases the number of Fe^{+3} sites in contact with the polymer and decreases the T_1 time constant. Figure 8 indicates that the Na^+ and 30B exchanged clay have a zero strain T_1 (~1.00 s) higher than the zero strain T_1 values (~0.70 s) of the 20A and 25A modified clay composites. The 20A and 25A modifications are nonpolar and more closely match the nonpolar structure of the polyisoprene, leading to more intercalation (Table I). Better dispersion and the lower zero strain values of the T_1 time constants are consistent with more Fe^{+3} exposure to the polyisoprene. This increased exposure means fewer unexposed paramagnetic centers prior to compression. As a result, there is no significant increase in interactions between the polymer and the clay when the composite is compressed. Thus, as seen in Figure 8, there were no significant changes in the spin–lattice relaxation time constants with increased strain for the 20A and 25A modifications.

More interactions between the polymer and filler and better dispersion would be expected to produce an improvement in modulus of the samples.[9] Figure 9 shows clearly, however, that the compression modulus decreased meaningfully for the two samples con-

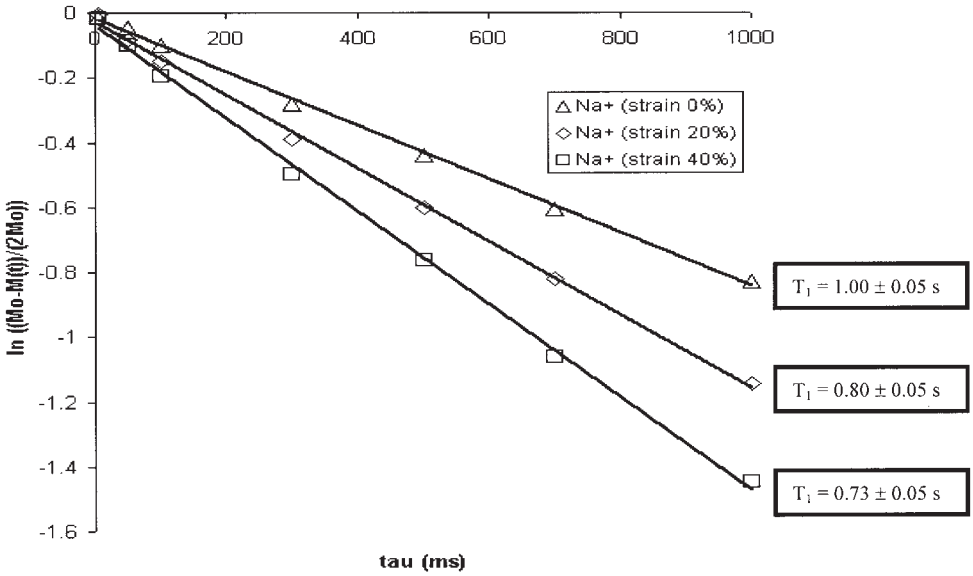

Figure 6 Magnetization recovery curve for *cis* 1,4-polyisoprene nanocomposites containing 13 wt % Na^+ exchanged clay under compressive strains at −10 °C.

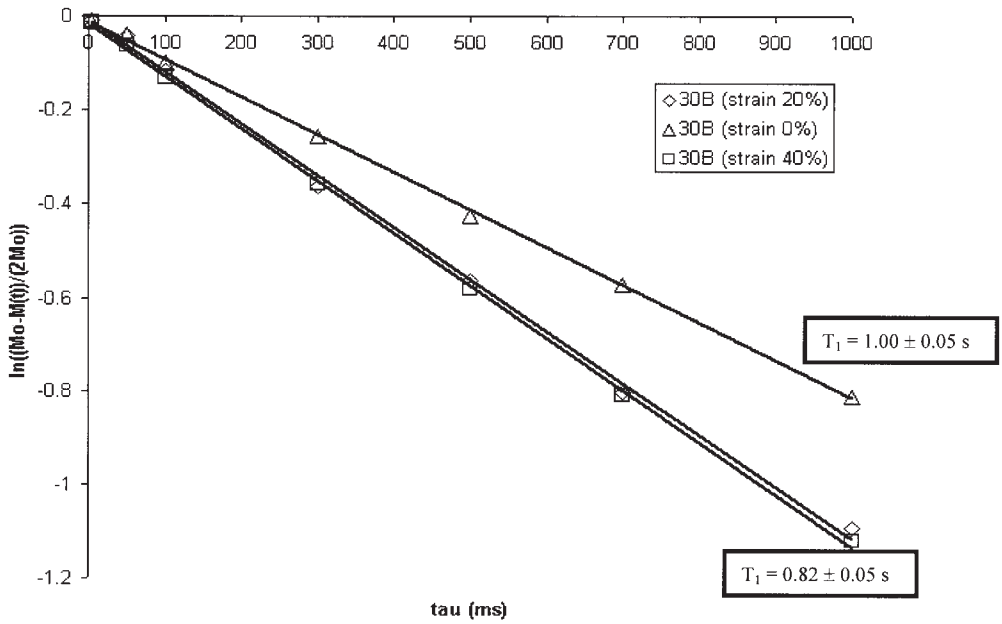

Figure 7 Magnetization recovery curve for *cis* 1,4-polyisoprene nanocomposites containing 13 wt % 30B exchanged clay under compressive strains at −10 °C.

taining the more compatible 20A and 25A surfactants. The reason for this decrease lies in the anisotropic composite nature of the effective filler particle when clay tactoids are present. There are substantial differences in the mechanical response of clay-filler elastomers compared to more traditional carbon black filled compounds. In the latter, favorable filler–polymer interactions lead to bound and occluded rubber, which adds to the effective volume filling capacity of the irreducible and nondeformable carbon black aggregates, thereby enhancing the modulus. Intercalated clay tactoids are anisotropic and deformable; the amount of readily sheared material in the interlamellar galleries, dependent on surfactant modification, directly influences the soft shearing modes of deformation of the anistropic tactoids. Thus, in the more compatible 20A and 25A blends, the ease of the tactoid shearing overcompensates for any reinforcing effects of the filler and the modulus decreases. It is also important to point out that better compatibility of surfactant and matrix polymer should lead to an increased fraction of exfoliated clay sheets. As discussed in detail in a previous publication,[30] these exfoliated sheets do not augment the modulus as effectively as a particle containing several clay sheets. Reasons for this nonreinforcing property of clay fillers include the very low value of effective volume fraction per unit weight of clay when an isolated surfactant-modified clay

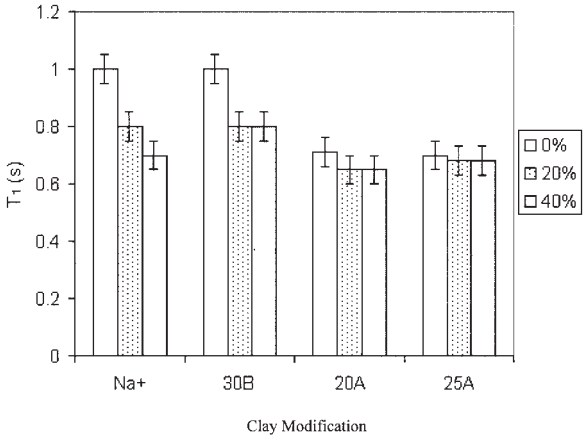

Figure 8 T_1 time constants of *cis* 1,4-polyisoprene–montmorillonite nanocomposites under compressive strains at −10 °C.

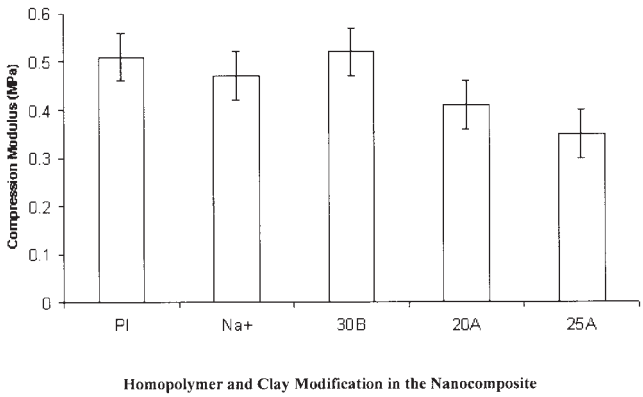

Figure 9 Compression modulus for *cis* 1,4-polyisoprene and *cis* 1,4-polyisoprene–montmorillonite nanocomposites.

layer is considered. In addition, there is a tendency for exfoliated clay sheets to adopt easily deformed curved configurations in a polymer matrix.

Continuation of this work focused on the use of magic angle spinning to resolve the three chemically distinguishable protons on polyisoprene and independently monitor changes in their interactions with the clay interface. There were no differences among the interactions experienced by all three types of protons. Furthermore, confirming our results from the static spectra, increases in interfacial area were observed with an increase in compressive strain. Application of the magic angle spinning technique for compressed nanocomposites will be the focus of future publications.

CONCLUSIONS

Solid-state NMR, through measurements of spin–lattice relaxation times, can be used to quantify the strain-dependent evolution of interfacial area in clay–polyisoprene nanocomposites. Strain-induced evolution of interfacial area is dependent on the surfactant employed and therefore the initial amount of intercalation by the polymer. In the clay-filled samples, soft modes of tactoid deformation compensated for any reinforcing effect of the filler. In this case, with the more highly intercalated tactoids, a statistically significant reduction in the modulus was observed.

The authors acknowledge the Center of Material Science (MIT-CMSE) for use of their microscopy and X-ray scattering facilities. Special thanks are extended to Professor Jeff Abes for assistance with TEM.

References

1. Kim, G. M.; Lee, D. H.; Hoffmann, B.; Kressler, J.; Stoppelmann, G. Polymer 2001, 42, 1095.
2. Tucker, H. Encyclopedia of Chem Technology, 3rd ed.; Wiley: New York, 1979.
3. Tobolsky, A. V.; Prettyman, I. B.; Dillon, J. H. J Appl Phys 1944, 15, 380.
4. Mooney, M.; Wolstenhdue, W. E.; Villars, D. S. J Appl Phys 1944, 15, 324.
5. Choi, I. S.; Roland, C. M. Rubber Chem Technol 1997, 70, 202.
6. Razumovski, S. D.; Podmastevev V. V.; Zaikov, G. E. Polym Degrad Stabil 1988, 20, 37.
7. Matsumiya, Y.; Watanabelt, K.; Osaki, K. Macromolecules 1999, 32, 6734.
8. Clarke, S. M.; Elias, F.; Terentjev, E. M. Eur Phys J E 2000, 2, 335.
9. Lincoln, D. M.; Vaia, R. A.; Wang, Z. G.; Hsiao, B. S. Polymer 2001, 42, 1621.
10. Menge, H.; Hotopf, S.; Heuert, U.; Schneider, H. Polymer 2000, 41, 3019.
11. Loo, S. S.; Cohen, R. E.; Gleason, K. K. Macromolecules 1998, 31, 8907.
12. Hedden, R.C.; McCasey, E.; Cohen, C.; Duncan, T. M. Macromolecules 2001, 34, 3285.
13. McLoughlin, K.; Waldbieser, J. K.; Cohen, C.; Duncan, T. M. Macromolecules 1997, 30, 1044.
14. Vu, Y. T.; Mark, J. E.; Pham, L. H.; Engelhardt, M. J Appl Polym Sci 2001, 82, 1391.
15. Okada, A.; Usaki, A. Mater Sci Eng 1995, C3, 109.
16. Bala, P.; Samantaray, B. K.; Svivastava, S. K.; Nando, G. B. J Appl Polym Sci 2004, 92, 3583.
17. VanderHart, D. L.; Asano, A.; Gilman, J. W. Chem Mater 2001, 13, 3796.
18. VanderHart, D. L.; Asano, A.; Gilman, J. W. Macromolecules 2001, 34, 3819.
19. Zax, D. B.; Yang, D. K.; Santos, R. A.; Hegemann, H.; Giannelis, E. P.; Manias, E. J Chem Phys 2000, 112, 2945.
20. Bruch, M. D. NMR Spectroscopy Techniques; Dekker: New York, 1996.
21. Personal communication with Southern Clay Products representative.
22. Bloembergen, N.; Morgan, L. O. J Chem Phys 1961, 34, 842.
23. Henrichs, P. M.; Cofield, M. L.; Yound, R. H.; Hewitt, J. M. J Magn Reson 1984, 58, 85.
24. Abragam, A. Principles of Nuclear Magnetic Resonance; Oxford University Press: Oxford, 1961.
25. English, A; Dybowski, C. R. Macromolecules 1984, 17, 447.
26. Labouriau, A.; Kim, Y.; Earl, L. Phys Rev B 1996, 54, 9952.
27. Bryar, T. R.; Daughney, C. J.; Knight, R. J. J Magn Reson 2000, 142, 74.
28. Nestle, N.; Zimmermann, C.; Dakkouri, M.; Karger, J. J Phys D Appl Phys 2002, 35, 166.
29. Klempt, T.; Kanert, O.; Suter, D. Phys Stat Sol B 2003, 236, 151.
30. Sheng, N; Boyce, M. C.; Parks, D. M.; Rutledge, G. C.; Abes, J. I.; Cohen, R. E. Polymer 2004, 45, 487.